Operando study on wet CO oxidation over ceria and alumina supported platinum catalysts

Downloaded from: https://research.chalmers.se, 2026-11-18 17:49 UTC

Citation for the original published paper (version of record):
Di, M., Schaefer, A., Hemmingsson, F. et al (2026). Operando study on wet CO oxidation over ceria and alumina supported platinum catalysts. Applied Catalysis O: Open, 219.
http://dx.doi.org/10.1016/j.apcato.2026.207113

N.B. When citing this work, cite the original published paper.

research.chalmers.se offers the possibility of retrieving research publications produced at Chalmers University of Technology. It covers all kind of research output: articles, dissertations, conference papers, reports etc. since 2004. research.chalmers.se is administrated and maintained by Chalmers Library

(article starts on next page)

Applied Catalysis O: Open 219 (2026) 207113

Contents lists available at ScienceDirect

Applied Catalysis O: Open

journal homepage: www.elsevier.com/locate/apcato

Operando study on wet CO oxidation over ceria and alumina supported platinum catalysts☆

Mengqiao Di [a], Andreas Schaefer [a], Felix Hemmingsson [a], Tamsin Bell [b], Yanyue Feng [a], Magnus Skoglundh [a], David Thompsett [b], Per-Anders Carlsson [a,*]

[a] Competence Centre for Catalysis, Department of Chemistry and Chemical Engineering, Chalmers University of Technology, 412 96 Gothenburg, Sweden
[b] Johnson Matthey Technology Centre, Blounts Court, Sonning Common, Reading, RG4 9NH, UK

ARTICLE INFO

Keywords:
Low-temperature activity
Water promotion
Active ionic platinum
Mars-van Krevlen mechanism
Operando infrared spectroscopy

ABSTRACT

The effect of water on carbon monoxide oxidation activity of highly dispersed Pt/ceria and Pt/alumina catalysts with narrow Pt particle size distributions at around 1–2 nm has been studied by kinetic measurements and infrared spectroscopic characterisation under *in situ* and *operando* conditions. Water promotes the low-temperature activity for both catalysts, however, by different mechanisms. For Pt/ceria, the reaction proceeds with a very weak dependence on water concentration whereas the apparent activation energy increases. It is proposed that water, on the one hand, promotes the Mars-van Krevelen mechanism through destabilisation of ceria lattice oxygen favouring its reaction with CO and/or desorption of product CO_2 and, on the other hand, turn ionic Pt clusters active for CO oxidation. For Pt/alumina, the CO oxidation proceeds via Langmuir–Hinshelwood mechanism on Pt, however, with a positive dependency on water concentration. Likely water both weakens the interaction between CO and Pt, and may enable the proposed reaction pathway between CO and OH ad-species to form surface carboxylates as part of a wet CO oxidation mechanism.

1. Introduction

Water interacts with nearly all solid surfaces, and heterogeneous catalysts are no exception. When water is adsorbed on the catalyst sites, it affects the catalytic functions, and thus often the overall catalytic efficiency. Water can be an inhibitor, a promoter, a cocatalyst or a reactant [1]. For example, water inhibits lean methane oxidation over alumina-supported palladium catalysts [2,3], which to some extent can be counteracted by using another support [4]. In the water–gas shift reaction over platinum supported by ceria, water is obviously a reactant [5]. Furthermore, water significantly suppresses the oxidation of carbon monoxide (CO) over metal oxides [6,7] while for ideal surfaces of noble metals (Pd, Pt, and Au), water has been reported to promote the catalytic activity for the oxidation of CO at low temperatures [8–10]. Water is also known to promote the oxidation of CO on platinum supported by ceria and alumina [11,12]. Additionally, the presence of water has been shown to affect the dispersion of supported Ru and Rh particles through disruptive breaking of metal–metal bonds [13,14]. Compared with ideal surfaces, these systems are structurally richer, involving the complexity of platinum nanoparticles and clusters, and their delicate interaction with the support, which contributes to their catalytic properties.

In previous work, we investigated in detail the CO oxidation over highly dispersed Pt/ceria and Pt/alumina catalysts synthesised by industrially relevant methods under dry conditions [15] and in the presence of nitrogen oxide (NO) [16]. Concerning the physicochemical properties of the catalysts, the platinum loading was measured by X-ray fluorescence to be 1.09 and 1.92 wt% for the alumina and ceria supported catalyst, respectively. Both catalysts consist of small Pt nanoparticles, around 1–2 nm based on CO chemisorption, but also smaller clusters as evidenced by transmission electron microscopy. The mean platinum particle size was 1.0 and 1.3 nm for the ceria and alumina catalysts, respectively. With X-ray diffraction, only reflections caused by the supports were detectable. Hydrogen temperature programmed reduction experiments for the Pt/alumina catalyst showed peaks at 76, 212 and 379 °C with hydrogen consumption of 0.035, 0.08 and 0.2 mmol/g_{cat}, respectively. The low temperature peak was associated with surface reduction of larger Pt particles, while the high temperature peak was assigned to reduction of oxidised Pt particles whose state is significantly stabilised by the alumina support. In the case of Pt/ceria, peaks were observed at 77 and 120 °C corresponding to hydrogen consumption of 0.4 and 0.15 mmol/g_{cat}, respectively. The

☆ This article is part of a Special issue entitled: 'Operando Catalysis' published in Applied Catalysis O: Open.

* Corresponding author.
E-mail address: per-anders.carlsson@chalmers.se (P.-A. Carlsson).

https://doi.org/10.1016/j.apcato.2026.207113
Received 23 June 2026; Received in revised form 13 August 2026; Accepted 30 August 2026
Available online 17 September 2026
2950-6484/© 2026 The Authors. Published by Elsevier B.V. This is an open access article under the CC BY license (http://creativecommons.org/licenses/by/4.0/).

low-temperature peak was assigned to reduction of platinum oxides but also ceria lattice oxygen close to the particle rim as the nominal consumption in the case of complete reduction of Pt^{4+} was 0.1 mmol/g_{cat}. The peak at higher temperature was assigned to reduction of ceria lattice oxygen farther away from the Pt species as a result of hydrogen migration. By *operando* DRIFTS, the CO ad-species were identified. For the Pt/ceria catalyst, CO linearly adsorbed on ionic platinum (Pt^{2+}) and partially oxidised platinum ($Pt^{\delta+}$) gave rise to IR signatures at 2107 and 2078 cm^{-1}, respectively. Interestingly, the CO bonded to ionic Pt was identified to be a spectator species. By correlating the infrared results with *operando* X-ray absorption spectroscopy results, the oxidation activity for Pt/ceria at low temperatures, i.e., below the light-off temperature, was shown to originate from a Mars-van Krevelen (MvK) mechanism involving ceria lattice oxygens, which is in line with our theoretical predictions [17]. Upon co-feeding of NO, the light-off temperature increases because the MvK mechanism is suppressed by the formation of nitrates that block the otherwise accessible lattice oxygen from participating in the CO oxidation. This is different from the case of Pt/alumina, for which the oxidation of CO proceeds through a Langmuir–Hinshelwood (LH) mechanisms on the Pt particles [18].

Here we expand the knowledge about these catalysts by exploring how water, either cofed or pre-adsorbed, influences the CO oxidation and how wet CO oxidation conditions affect catalyst morphology. To this end, we used a combination of kinetic measurements, a number of *ex situ* characterisation techniques applied to the spent catalysts as well as *in situ* and *operando* infrared spectroscopy.

2. Experimental

The catalyst preparation and basic characterisation of the as-prepared platinum ceria and platinum alumina catalysts are described in previous work [15]. In short the catalysts were prepared by incipient wetness impregnation using platinum salts followed by drying and calcination at 500 °C in static air.

2.1. Basic characterisation of spent catalysts

The crystallinity of the spent catalysts, i.e., after being exposed to CO oxidation conditions w/wo water, was characterised by powder X-ray diffraction (PXRD) using a D8 Discover diffractometer (Bruker) equipped with a Cu-Kα X-ray source (1.5418 Å) and an EIGER2 R 500 K hybrid photon counting (HPC) detector. Diffracted X-rays were recorded under ambient conditions with a variable slit and a fixed sample illumination of 7 mm in the 2θ range from 20 to 91° with an incremental step of 0.02°. Each step was measured for 2 s.

The spent catalysts were imaged by high-resolution transmission electron microscopy (HRTEM) and scanning transmission electron microscopy (STEM) using a Tecnai T20 microscope (FEI), and a Titan 80-300 microscope (FEI), respectively. The Tecnai T20 microscope was equipped with a LaB_6 filament operated at 200 kV and a high-angle annular dark-field (HAADF) STEM detector. A field emission gun operated at 300 kV was used for the Titan 80-300 microscope. The specimen was prepared by dispersing the spent catalyst in ethanol using ultrasonication for enhanced mixing. A droplet of the obtained suspension was then applied to a holey carbon film supported on a copper grid. The recorded micrographs where analysed using ImageJ [19].

2.2. Catalytic tests and reaction order measurements

The catalyst performance was evaluated using a stainless steel fixed-bed powder reactor, as described in detail elsewhere [20], positioned in a vertical flow direction. In brief, the sample was placed in the 4 mm wide and 16 mm long sample compartment, and a type K thermocouple was located 2 mm into the sample bed. The reactor was heated resistively by an inbuilt heating coil using a PID regulator and another type K thermocouple for measuring the reactor block temperature. The entire reactor was insulated. The feed gas composition was composed by a set of mass flow controllers (Bronkhorst). The effluent gas was analysed using a mass spectrometer (Pfeiffer Vacuum GSD-350) following the m/e ratios: 2 (H_2), 18 (H_2O), 28 (CO), 32 (O_2) and 44 (CO_2).

The powder samples were sieved and the fraction 100–300 μm was kept and diluted with cordierite, which had been ground and sieved to the same fraction. Around 10 mg of catalyst was mixed with 90 mg ground cordierite, and then loaded into the reactor.

Catalytic performance tests were carried out using 0.2 vol.% CO, 1.0 vol.% O_2 w/wo 2.0 vol.% H_2O. The total flow was 150 ml/ min and constant, and Ar was used as a carrier gas throughout the measurements. The reactor temperature was first increased from room temperature to 350 °C with a rate of 5 °C/ min and then dwelled for one hour in the reaction mixture. Then a catalytic extinction–ignition cycle was repeated three times where the reactor temperature was decreased from 350 to 35 °C, held constant for 10 min, increased to 350 °C and finally held constant for 30 min, before repeating the next two extinction–ignition cycles. Additional catalytic activity tests in with pre-adsorbed water (2 vol.% H_2O, 2 h, 35 °C) were also carried out. After purging in Ar for 1 h, the catalytic ignition was then followed by increasing the reactor temperature to 350 °C with a rate of 5 °C/ min. Based on previous characterisation of number of platinum surface atoms [15], the turn-over frequency (TOF) was calculated from the ignition data at 75 °C, which represents the kinetic regime for all catalysts.

Reaction order measurements for CO oxidation with respect to O_2, CO and H_2O were performed. Prior to the O_2 reaction order measurements, the Pt/ceria sample was treated with 0.2 vol.% CO for 1 hr at 35 °C before introducing 2 vol.% H_2O and 1 vol.% O_2 at 45 °C for 1 hr. Then the O_2 concentration was increased in steps from 1.4 to 2.5 vol.% at 45 °C, and kept constant for 30 min at each step. Similarly, for the Pt/alumina sample, the O_2 concentration was varied in the range of 1 to 2.1 vol.% in the presence of 0.2 vol.% CO and 2 vol.% H_2O at 127 °C. Concerning the CO reaction order measurements, the Pt/ceria sample was first exposed to 2 vol.% H_2O and 1 vol.% O_2 at 35 °C for one hour. Then the CO concentration was increased in steps in the range 0.1 to 0.25 vol.% at 45 °C. The CO reaction order for CO oxidation over the Pt/alumina sample was measured in the CO range from 0.16 to 0.25 vol.% in the presence of 2 vol.% of H_2O and 1 vol.% of O_2 at 127 °C. Each step was maintained for 30 min. Finally, for the water reaction order measurements, the Pt/ceria sample was pretreated with 0.2 vol.% CO for 1 h at 35 °C followed by the addition of 1 vol.% O_2 and 0.5 vol.% H_2O at 45 °C for 2 h. The H_2O concentration was increased in steps in the range from 0.8 to 2 vol.% H_2O at 45 °C. As for Pt/alumina, the H_2O concentration was increased in the range from 0.5 to 2 vol.% at 127 °C with a constant 1 vol.% O_2 and 0.2 vol.% CO. Each step was maintained for 30 min as to reach steady state.

2.3. Infrared spectroscopic characterisation

Diffuse reflectance infrared Fourier transform (DRIFT) spectroscopic speciation of adsorbates was done both under *operando* conditions and in *in situ* mode using a VERTEX 80v spectrometer (Bruker) equipped with a nitrogen-cooled MCT Photovoltaic 1 mm 8H detector and an evacuated optics bench to minimise interference from atmospheric components (water and carbon dioxide). A high-temperature stainless steel reaction chamber (Harrick Inc.) with CaF_2 windows was mounted inside a Praying Mantis mirror accessory (Harrick Inc.). One type K thermocouple was bent and inserted into the sample holder to measure the temperature of the catalyst bed and another thermocouple was placed underneath the sample holder for control of the reactor temperature.

For the measurements, around 55 mg of the Pt/ceria and 45 mg of the Pt/alumina catalyst were filled inside the sample holder. The feed gas was composed by individual mass flow controllers (Bronkhorst)

and a total gas flow of 100 ml/min was used. Ar was used as carrier gas in all measurements. IR spectra were collected in the range 4400–400 cm^{-1} with a spatial resolution of 1 cm^{-1}. Background spectra were recorded by averaging 100 scans, and sample spectra were then collected by scanning 50 times using a 6 mm aperture and 20 kHz scanner velocity.

The first type of DRIFTS measurement focused on the wet CO oxidation. The catalyst sample was pretreated by heating to 211 °C during exposure to 5 vol.% O_2 for 40 min followed by 2.0 vol.% H_2 for 30 min, and thereafter to pure Ar for at least 2 h until low and stable water levels were measured in the effluent stream. Then, the temperature was decreased in steps to 35 °C and a background spectrum was recorded at each temperature. The wet CO oxidation experiments were started by introducing 0.2 vol.% CO, 1.0 vol.% O_2 and 2.0 vol.% H_2O (added using a water vapour generator described elsewhere [21]) at 35 °C for 2 h. Then the temperature was increased in steps to 211 °C followed by a stepwise decrease back to 35 °C. Each spectrum was acquired after about 10 min when the set temperature had been reached and the corresponding background spectrum recorded at the same set temperature was then subtracted.

The second type of DRIFTS measurement was CO adsorption on water pre-treated catalysts followed by desorption of CO. The same pretreatment and background collection procedures as for wet CO oxidation were used. The sample was exposed to 2.0 vol.% H_2O for 2 h and then to 0.2 vol.% CO for another 2 h at 35 °C. Time-resolved spectra were collected at 35 °C for 2 h with a time interval of 10 min. Then the temperature was increased in steps to 212 °C and spectra collection was made as for the wet CO oxidation.

The third type of DRIFTS measurement was CO oxidation over water pre-treated catalysts. Again, the same pretreatment and background collection procedures as for wet CO oxidation were used. The sample was exposed to 2 vol.% H_2O for 2 h. Then 0.2 vol.% CO and 1.0 vol.% O_2 were introduced at 35 °C for another hour, and time-resolved spectra were recorded with a 10 min time interval. Then the temperature was increased in steps to 212 °C and spectra collection was made as for the wet CO oxidation.

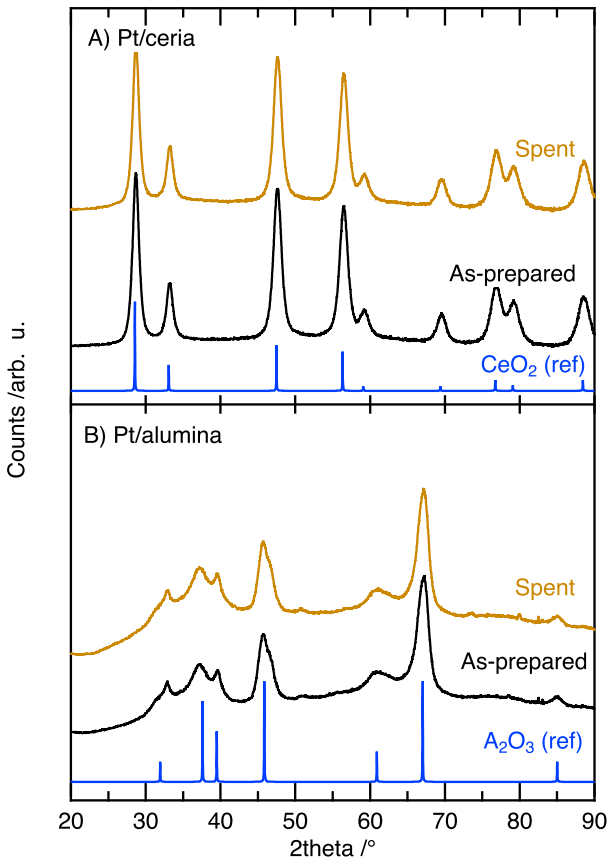

Fig. 1. XRD patterns of the as-prepared and spent, i.e., after dry and wet CO oxidation, Pt/ceria (panel A) and Pt/alumina (panel B) catalysts. The reflections are assigned using reference patterns (blue) from the Powder Diffraction File™ (PDF) database for cubic CeO_2 (PDF 00-004-0593) and γ-Al_2O_3 (PDF 00-010-0425).

3. Results

3.1. Diffraction and electron microscopy analyses

Fig. 1 shows the X-ray diffractograms of the spent Pt/ceria and Pt/alumina catalysts, i.e., after dry and wet CO oxidation. Diffractograms for as-prepared catalysts are included for comparison and the patterns for γ-alumina (PDF 00-010-0425) and CeO_2 cubic fluorite structure (PDF 00-004-0593) are included for reference. The diffractograms of the spent catalysts are identical to the corresponding ones of the as-prepared catalysts. Further, the diffractogram of the Pt/ceria and Pt/alumina sample matches the reference pattern of fluorite CeO_2 and γ-alumina, respectively. The apparent support crystallite size was calculated by using the Sherrer equation. The ceria crystallite size is found to be 7 nm for both the as-prepared and spent catalysts. Likewise, the alumina crystallite size for the as-prepared and spent Pt/alumina samples after CO oxidation with H_2O is determined to be 6 nm. The diffractograms present no observable peaks for Pt phases.

The support crystallite sizes can also be estimated from the TEM images shown in the left column of Fig. 2 (panels A and D). Here, the size of the spent ceria and alumina crystallites is around 7 and 10 nm, respectively. Concerning the Pt phase, TEM imaging is superior to present PXRD for analysis of the small Pt particles. In addition to TEM images, Fig. 2 displays STEM images (panels B and E) and estimated particle size distributions (PSD) (panels C and F) for the spent Pt/ceria and spent Pt/alumina catalysts. The Pt particles appear somewhat diffuse in the TEM images in part due to the small difference in mass between Pt and Ce, and in part, because low mass-thickness contrast originating from thickness variations in the specimen. Nevertheless, the observed fringes are indicative of a superposition of different types of crystal planes oriented in different directions. In the STEM images, however, the Pt particles can be clearly distinguished from the ceria support thanks to the difference in atomic number. Concerning the PSD for Pt/ceria after CO oxidation with H_2O, the majority of the Pt particles fall within the range of 0.5–1.3 nm, with a mean Pt particle size of 1.1 nm based on 265 particles as for the as-prepared catalyst [15]. For the spent Pt/alumina sample, the majority of the Pt particles falls within the range of 0.7–2.5 nm with a mean particle size of 1.6 nm based on 585 particles.

3.2. Flow-reactor analysis

The measured CO conversions profiles during extinction and ignition (third cycle) for CO oxidation in dry and wet conditions for Pt/ceria and Pt/alumina, are shown in Fig. 3A and B, respectively. The CO conversions for the ignition process in the case of pre-adsorbed H_2O are shown as well.

Starting with the Pt/ceria catalyst, it is clear that the hysteresis between the conversion profiles for extinction and ignition shifts towards lower temperatures for wet CO oxidation as compared to dry conditions. During ignition, the light-off temperature, here denoted with T_{50}^{ig} signifying 50% CO conversion, decreases from 155 °C for dry CO oxidation to 114 °C for wet conditions. As for the extinction process, the corresponding T_{50}^{ex} decreases from 145 °C for dry CO oxidation to 99 °C for wet oxidation. The temperature difference, i.e., T_{50}^{ig} - T_{50}^{ex}, is 10 °C for dry CO oxidation, and slightly larger, 15 °C, for wet conditions. The

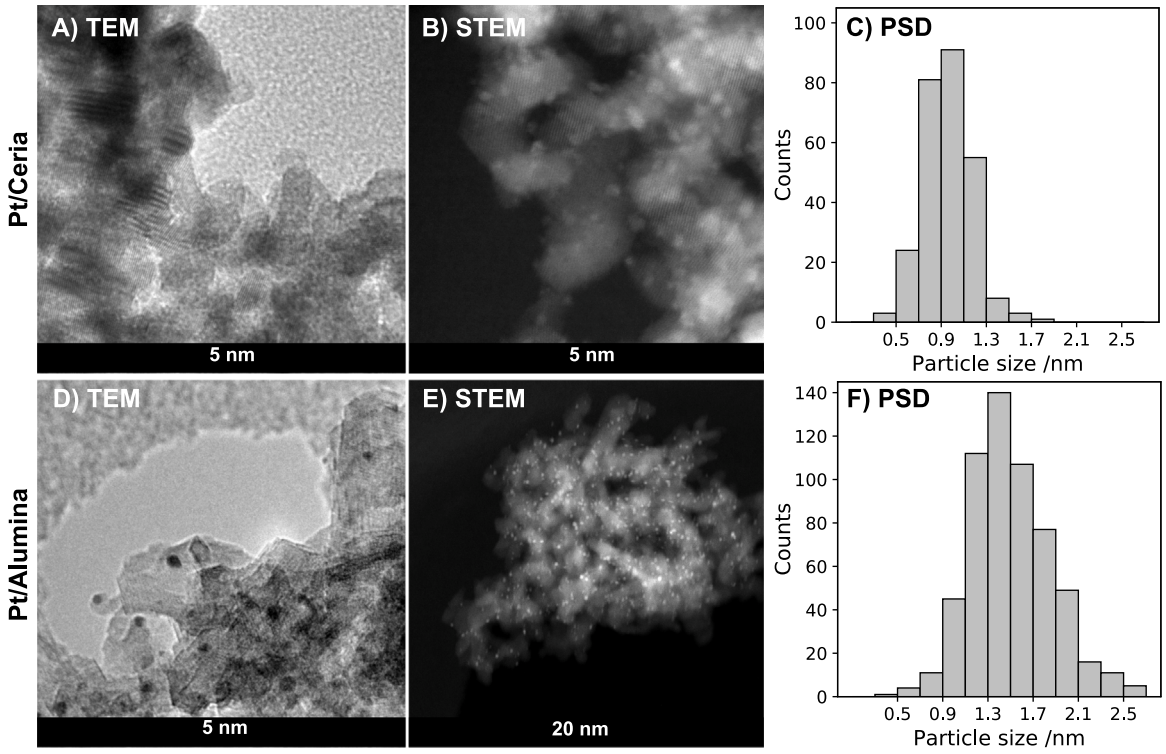

Fig. 2. High-resolution TEM (panel A) and STEM-HAADF (panel B) micrographs as well as platinum particle size distribution (panel C) of the spent Pt/ceria catalyst. Panels D-F show the corresponding results for the spent Pt/alumina. For the spent Pt/ceria catalyst, the average platinum particle size is 1.1 nm based on 265 Pt particles and for Pt/alumina catalyst the corresponding average size is 1.6 nm based on 585 particles.

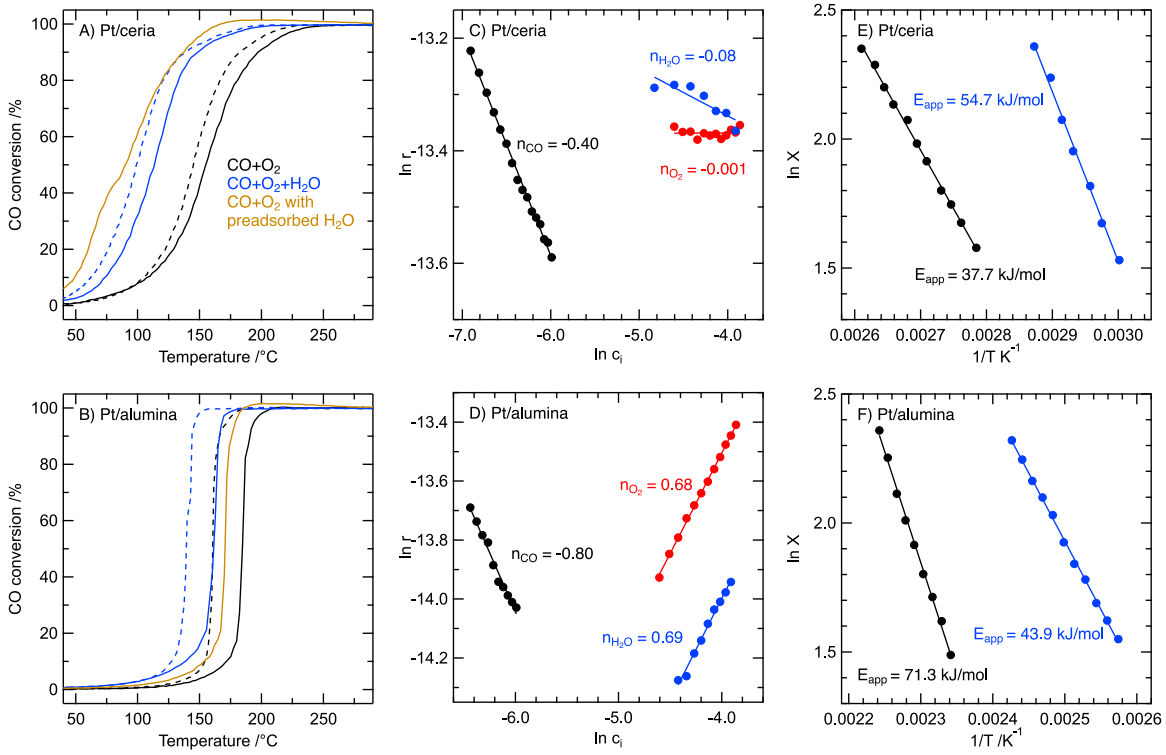

Fig. 3. Panels A and B show ignition (solid lines) and extinction (dashed lines) profiles for dry CO oxidation with 0.2 vol.% CO and 1.0 vol.% O_2 (black), with the addition of 2.0 vol.% H_2O (blue), and with pre-adsorbed H_2O (brown). Panels C and D show CO, O_2 and H_2O concentration dependencies of the CO oxidation reaction rate (mol CO_2 g^{-1} s^{-1}) over Pt/ceria performed at 45 °C and Pt/alumina at 127 °C. Panels E and F show Arrhenius plots for dry (black) and wet (blue) CO oxidation conditions. The reaction orders and apparent activation energies were obtained by linear fitting of data obtained at low (< 10%) CO conversion whereof the latter was fitted to ignition data.

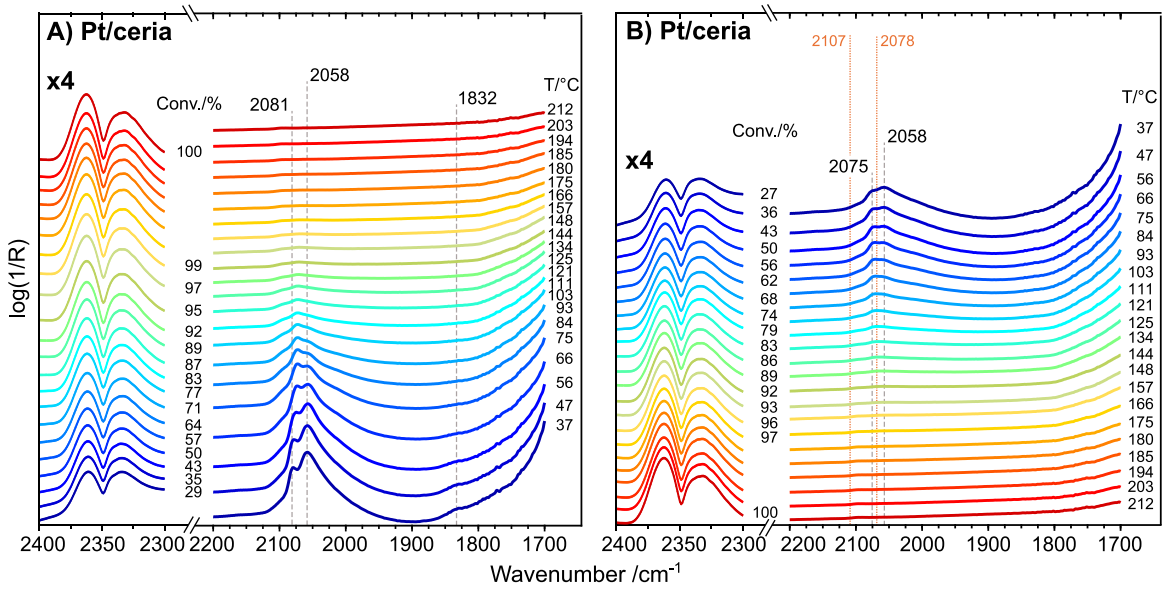

Fig. 4. *Operando* infrared difference spectra (hydrogen treated sample as reference) collected at indicated sample temperatures while increasing (panel A) and decreasing (panel B) the sample temperature in steps in the presence of 0.2 vol.% CO, 1 vol.% O_2 and 2 vol.% H_2O (Ar as balance). The measured global CO conversion is indicated at each temperature. The vertical orange dashed lines in panel B indicate peak positions previously observed in dry conditions [15].

effect of pre-adsorbed H_2O on the CO conversion is similar in the cases of continuous supply. It is noticeable that a CO conversion of around 5% is achieved at 35 °C and the T_{50}^{ig} is 90 °C, which is even lower than that of co-feeding of H_2O. The TOF at 75 °C is 0.015 and 0.049 s^{-1} for dry and wet conditions, respectively.

Moving to the Pt/alumina catalyst, the CO conversion profiles during the catalytic extinction–ignition measurements exhibit a sudden change in the CO conversion at low temperatures in stark contrast to the Pt/ceria catalyst. The T_{50}^{ex} and T_{50}^{ig} for dry CO oxidation occur at 161 °C and 185 °C, respectively. Furthermore, T_{50}^{ex} decreases from 161 to 139 °C during wet conditions. As for the ignition, T_{50}^{ig} decreases from 185 to 161 °C in wet conditions. In contrast to Pt/ceria, no significant changes of the width of the hysteresis, i.e., T_{50}^{ig} - T_{50}^{ex}, can be observed. The difference is 24 and 22 °C for dry and wet CO oxidation, respectively. For the ignition following pre-adsorption of H_2O, the T_{50}^{ig} turns out to be 171 °C, which is lower than for dry conditions but higher than for wet CO oxidation. The TOF at 75 °C is 0.0008 and 0.0045 s^{-1} for dry and wet conditions, respectively.

The results for the reaction order measurements with respect to CO, O_2 and H_2O over Pt/ceria and Pt/alumina are displayed in Fig. 3C and D, respectively. Each reaction temperature was chosen as to balance reliable CO conversion measurements and sufficiently low conversion (below 20%) such that reaction rates are controlled by surface kinetics. For the Pt/ceria, the CO, O_2 and H_2O reaction orders are measured to be −0.39, 0.0013 and −0.08, respectively. As for Pt/alumina, the corresponding reaction orders are −0.84, 0.68 and 0.25. Apparent activation energy was also extracted in the low conversion regime as shown in panel E and F. For Pt/ceria the apparent activation energy is 37.7 and 54.7 kJ/mol for dry and wet conditions, respectively. The corresponding values for Pt/alumina is 71.3 and 43.9 kJ/mol.

3.3. Infrared spectroscopic speciation

Figs. 4 and 5 show the *operando* infrared difference spectra for ignition and extinction of wet CO oxidation over Pt/ceria and Pt/alumina, respectively. The temperature at which each spectrum was collected is indicated as is the corresponding global CO conversion measured with mass spectrometry.

Starting with the ignition experiment for the Pt/ceria catalyst (panel a), the double IR absorption band around 2350 cm^{-1} shows the product CO_2 in the gas phase. It is denoted by $\tilde{\nu}_{gas}^{CO_2}$, which is the notation style to be used hereafter for identified species. The $\tilde{\nu}_{gas}^{CO_2}$ band is obvious already from the beginning of the measurement at 37 °C, for which the CO conversion is 29%. Moving to the bands that signify surface species, the two major peaks at 2081 and 2058 cm^{-1} are assigned to CO adsorbed atop on partially oxidised platinum, $\tilde{\nu}_{lin}^{CO}(Pt^{\delta+})$, and zero valent platinum, $\tilde{\nu}_{lin}^{CO}(Pt^0)$, respectively [22,23]. The minor peak at 1832 cm^{-1} is assigned to CO bridge-bonded to zero valent platinum, $\tilde{\nu}_{br}^{CO}(Pt^0)$. With increasing temperature, the intensity of the $\tilde{\nu}_{gas}^{CO_2}$ band gradually increases while the bands for the CO ad-species decrease, also gradually. At 125 °C, the $\tilde{\nu}_{lin}^{CO}(Pt^0)$ band is hardly visible. At 134 °C, the position of the $\tilde{\nu}_{lin}^{CO}(Pt^{\delta+})$ band is redshifted by about 10 cm^{-1} from its starting position at 2081 cm^{-1}. At around 157 °C, all the peaks for CO ad-species are almost diminished and the CO conversion is 100%. Upon decreasing the temperature (panel b), the CO conversion slowly decreases to 89% at 134 °C and the intensity of the $\tilde{\nu}_{gas}^{CO_2}$ band decreases correspondingly. From here, the $\tilde{\nu}_{lin}^{CO}(Pt^{\delta+})$ and $\tilde{\nu}_{lin}^{CO}(Pt^0)$ bands start to grow, eventually resulting in peaks at 2075 and 2058 cm^{-1}, respectively. Compared to the ignition experiment, the position of the $\tilde{\nu}_{lin}^{CO}(Pt^0)$ band is the same while the $\tilde{\nu}_{lin}^{CO}(Pt^{\delta+})$ band is redshifted by 6 cm^{-1}.

Continuing with the ignition for the Pt/alumina catalyst (Fig. 5a), the IR band at 2085 cm^{-1} is assigned to $\tilde{\nu}_{lin}^{CO}(Pt^{\delta+})$ and the two bands at 2058 and 2044 cm^{-1} to $\tilde{\nu}_{lin}^{CO}(Pt^0)$ [18,24–26]. The latter two are more pronounced for Pt/alumina as compared to Pt/ceria. The peak at 1825 cm^{-1} is assigned to $\tilde{\nu}_{br}^{CO}(Pt^0)$ [18]. The $\tilde{\nu}_{gas}^{CO_2}$ band is hardly visible below 83 °C but when 94 °C is reached, its intensity increases abruptly and then increases gradually with increased temperature. The CO conversion also changes drastically from 22 to 73%. The intensities of the $\tilde{\nu}_{lin}^{CO}$ and $\tilde{\nu}_{br}^{CO}$ bands decrease when the temperature is increased from 36 to 94 °C and the band at 2058 cm^{-1} redshifts with about 7 cm^{-1}. When reaching 103 °C, the $\tilde{\nu}_{lin}^{CO}(Pt^0)$ band is minor and the $\tilde{\nu}_{br}^{CO}(Pt^0)$ band is completely vanished. At the highest temperature, no CO ad-species could be detected. With decreasing temperature (panel b), the $\tilde{\nu}_{gas}^{CO_2}$ band is rather intense until 103 °C is reached, from where it starts to decrease. At this temperature, the $\tilde{\nu}_{lin}^{CO}$ bands are visible, although their intensities are weak. At 83 °C, the intensity of the $\tilde{\nu}_{gas}^{CO_2}$ band and the CO conversion both drop. Concurrently, the intensities of the $\tilde{\nu}_{lin}^{CO}$ and $\tilde{\nu}_{br}^{CO}$ bands both increase clearly. At 64 °C, the $\tilde{\nu}_{gas}^{CO_2}$ band is hardly visible and the CO conversion is very low. From here a shoulder on the $\tilde{\nu}_{lin}^{CO}(Pt^0)$ band grows. During the initial growth of the $\tilde{\nu}_{lin}^{CO}(Pt^0)$ bands,

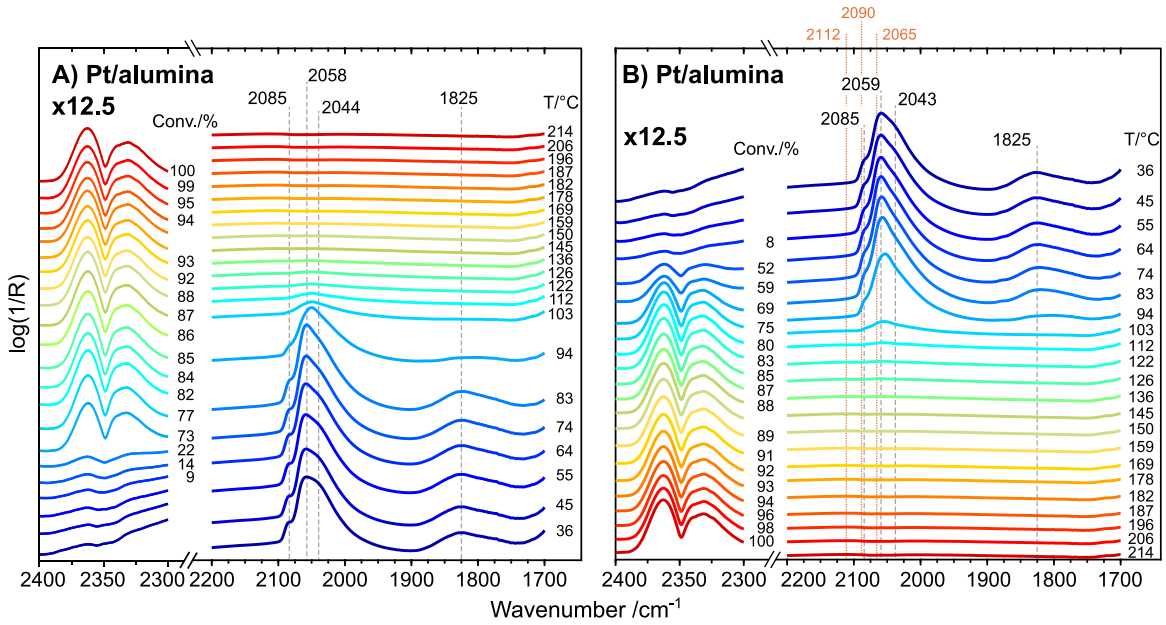

Fig. 5. *Operando* infrared difference spectra (hydrogen treated sample as reference) collected at indicated sample temperatures while increasing (panel A) and decreasing (panel B) the sample temperature in steps in the presence of 0.2 vol.% CO, 1 vol.% O_2 and 2 vol.% H_2O (Ar as balance). The measured global CO conversion is indicated at each temperature. The vertical orange dashed lines in panel B indicate peak positions previously observed in dry conditions [15].

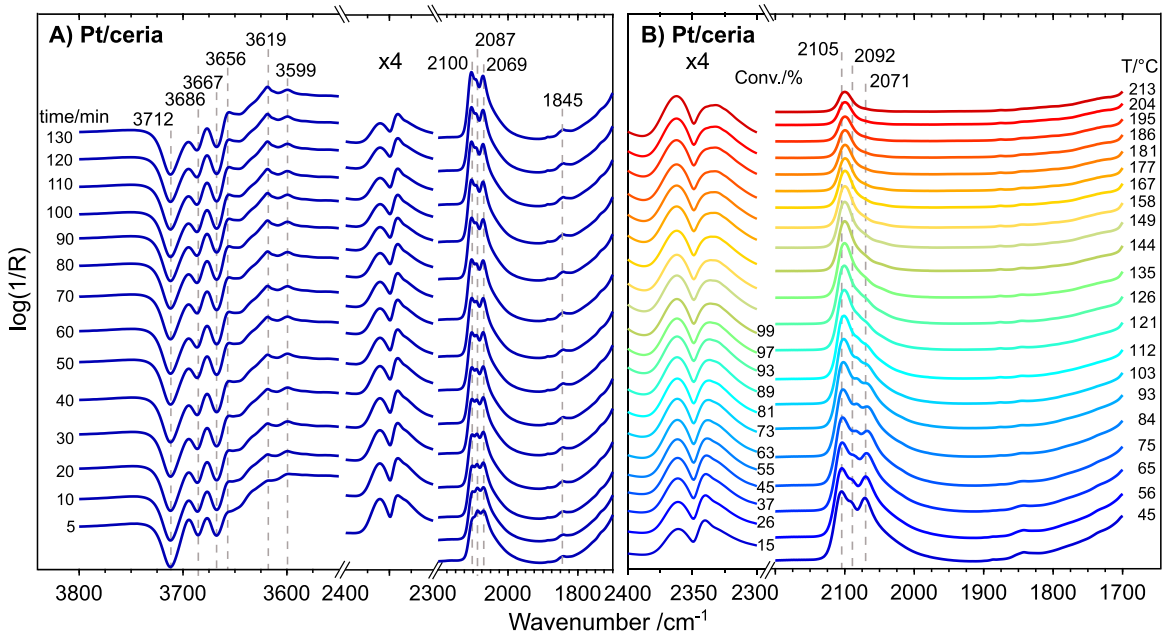

Fig. 6. Time-resolved infrared difference spectra collected *in situ* upon introduction of 0.2 vol.% CO and 1.0 vol.% O_2 (Ar as balance) at 35 °C to the Pt/ceria catalyst pre-exposed to 2.0 vol.% H_2O for 2 h (panel A) and subsequent *operando* infrared difference spectra collected during increasing temperature (panel B).

they also redshift by about 1-2 cm^{-1}. Upon further lowering of the temperature, their intensities increase and blueshifts by about 5 cm^{-1}.

Fig. 6 shows the time-resolved difference infrared spectra for CO oxidation at 35 °C over the Pt/ceria catalyst that has been pre-exposed to H_2O using the dry sample, i.e., pretreated in O_2, H_2 and Ar at elevated temperature as specified in the experimental section, as reference (panel a) followed by continued CO oxidation as a function of increased temperature (panel b). The negative peaks at 3712, 3686 and 3667 cm^{-1} are assigned to mono-coordinated hydroxyls, $\tilde{\nu}^{OH}_{mo}(Ce^{4+})$, non-dissociated water, $\tilde{\nu}^{H_2O}(Ce^{4+})$ and bridged hydroxyls, $\tilde{\nu}^{OH}_{br}(Ce^{4+})$, on ceria, respectively [27]. The positive peak at 3656 cm^{-1} can be assigned to bridged hydroxyl species on reduced ceria, $\tilde{\nu}^{OH}_{br}(Ce^{3+})$, and the two positive peaks at 3619 and 3599 cm^{-1} can be assigned to triple-bonded hydroxyls on ceria, $\tilde{\nu}^{OH}_{tr}(Ce^{4+})$ [28]. The band at 2100 cm^{-1} is assigned to CO adsorbed on ionic platinum, $\tilde{\nu}^{CO}_{lin}(Pt^{2+})$. As a function of time, the intensity of the $\tilde{\nu}^{OH}_{mo}(Ce^{4+})$ band decreases, while the intensity of the $\tilde{\nu}^{OH}_{br}(Ce^{3+})$ and $\tilde{\nu}^{OH}_{tr}(Ce^{4+})$ bands increases. This is even more clear in Supplementary Figure S1, which shows the difference between the first spectrum after introducing CO and the spectrum recorded in presence of H_2O (black spectrum) as well as the difference between the first and the last spectrum after introducing CO to the wet Pt/ceria sample (blue spectrum). From the black spectrum, for example, it is clear that the introduction of CO causes an intensity increase of the $\tilde{\nu}^{OH}_{br}(Ce^{3+})$ band at 3656 cm^{-1}. From the blue spectrum it is then clear that this band

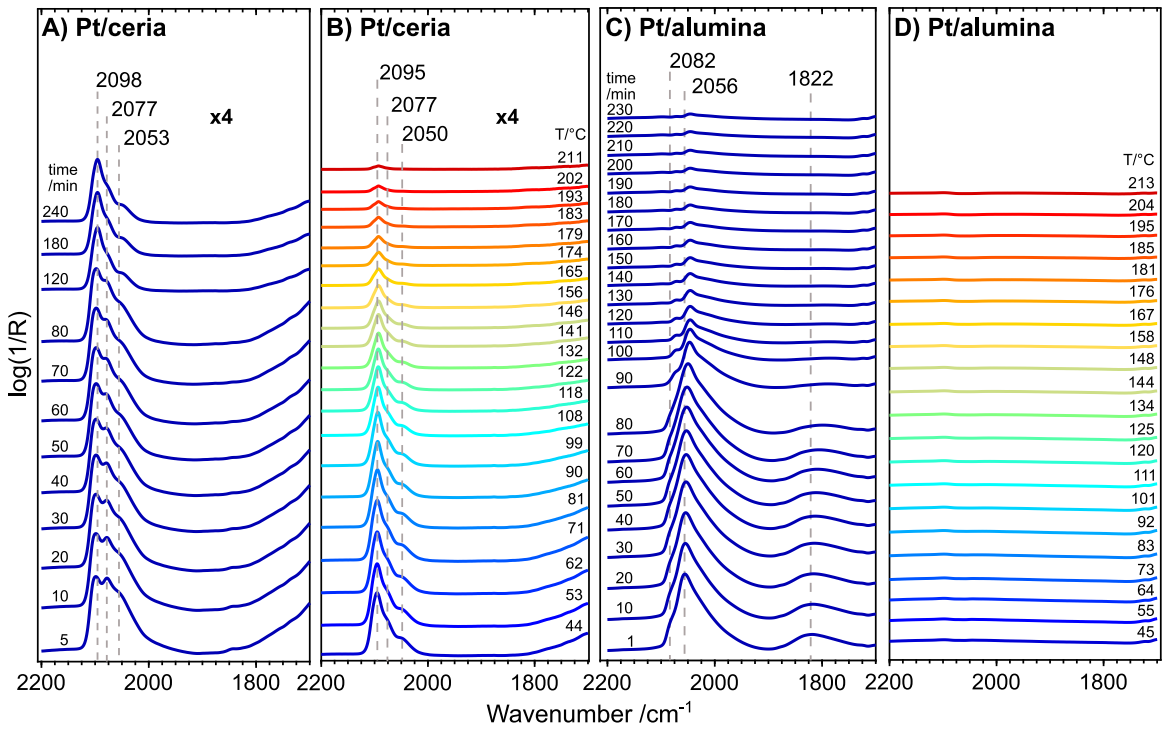

Fig. 7. *In situ* time-resolved infrared difference spectra collected at 35 °C upon introduction of 0.2% CO to the Pt/ceria (panel A) and Pt/alumina (panel C) catalysts that have been pre-exposed to H_2O for 2 h. Subsequent *in situ* infrared difference spectra collected during a step-wise increase of the temperature in Ar flow for Pt/ceria (panel B) and Pt/alumina (panel D).

increases in intensity even more as a function of time in presence of CO. This is accompanied by a gradual decrease in the intensity of the $\tilde{\nu}_{gas}^{CO_2}$ band. The intensities of the $\tilde{\nu}_{lin}^{CO}$ bands develop with a blueshift of about 5 cm^{-1} for the $\tilde{\nu}_{lin}^{CO}(Pt^{2+})$ and $\tilde{\nu}_{lin}^{CO}(Pt^{\delta+})$ bands, and around 2 cm^{-1} for the $\tilde{\nu}_{lin}^{CO}(Pt^0)$ band. Upon increasing the temperature, the intensity of the $\tilde{\nu}_{gas}^{CO_2}$ band gradually increases whereas the intensity of $\tilde{\nu}_{lin}^{CO}$ decreases. The $\tilde{\nu}_{lin}^{CO}(Pt^0)$ band immediately starts to decrease. Both the $\tilde{\nu}_{lin}^{CO}(Pt^0)$ and $\tilde{\nu}_{lin}^{CO}(Pt^{\delta+})$ bands redshift by 4 and 13 cm^{-1}, respectively. At 144 °C they are hardly visible and above this temperature, the CO conversion is 100%. The $\tilde{\nu}_{lin}^{CO}(Pt^{2+})$ band is visible also for the highest temperature of 213 °C.

In Fig. 7, the time-resolved infrared difference spectra collected at 35 °C upon introduction of 0.2% CO to the Pt/ceria (panel a) and Pt/alumina (panel c) catalysts that have been pre-exposed to H_2O for 2 h. For the Pt/ceria catalyst, the IR bands are of the same type as those observed during CO oxidation over the H_2O pre-exposed sample, although generally at lower wavenumbers. As a function of time on stream, the band intensities of $\tilde{\nu}_{lin}^{CO}(Pt^{2+})$, $\tilde{\nu}_{lin}^{CO}(Pt^{\delta+})$ and $\tilde{\nu}_{lin}^{CO}(Pt^0)$ decrease with a redshift of about 3 cm^{-1} from t= 5 min to t= 240 min. Upon increasing the temperature, the intensities of the $\tilde{\nu}_{lin}^{CO}(Pt^0)$ and $\tilde{\nu}_{lin}^{CO}(Pt^{\delta+})$ bands decrease and no clear bands can be discerned for temperatures above 179 °C and 183 °C, respectively. A minor $\tilde{\nu}_{lin}^{CO}(Pt^{2+})$ band can be seen 211 °C. As for Pt/alumina, the peaks at 2082 and 2056 cm^{-1} can be assigned to $\tilde{\nu}_{lin}^{CO}(Pt^{\delta+})$ and $\tilde{\nu}_{lin}^{CO}(Pt^0)$, respectively. The peak at 1822 cm^{-1} is assigned to $\tilde{\nu}_{br}^{CO}$. As a function of time on stream, the band intensities decrease. The $\tilde{\nu}_{lin}^{CO}(Pt^0)$ bands loses intensity while redshifting about 6 cm^{-1} during the first 80 min. At t = 90 min, a sudden decrease of the $\tilde{\nu}_{lin}^{CO}(Pt^0)$ band intensity occurs and the $\tilde{\nu}_{br}^{CO}$ band is almost vanished. No clear IR absorption bands can be seen after 230 min. When increasing the temperature, no further changes of the spectra are seen (panel d).

4. Discussion

4.1. Catalyst stability

The PXRD patterns and TEM images show that the crystallinity of both the ceria and alumina phases remains intact for the spent catalysts as compared to the as-prepared catalysts [15] described in the Introduction. Neither differences in crystallite size nor significant agglomeration of crystallites could be observed, so the supports are stable under the present conditions. Further, the STEM images show that no sintering of the Pt particles occurs for the Pt/ceria catalyst. The PSD is still narrow, and the mean particle size is 1.1 nm as compared to 1.0 nm before wet CO oxidation. The lack of reflections from Pt in the PXRD patterns suggests that the majority of the Pt crystallites are too small and/or amorphous to give clear diffraction peaks. [29,30]. For the spent Pt/alumina catalyst, a slight increase in the Pt particles size may be discerned. The mean platinum particle size increases from 1.3 to 1.6 nm. One cannot fully exclude the possibility that part of the small differences in the PSDs are influenced by the choice of region of interest during STEM imaging, although this is likely a minor issue. For example, the lack of visible peaks for Pt in the PXRD patterns indicates that Pt still exists in small particles and clusters after being used for reactions, which support the interpretation of the STEM images. All together, the morphology of both spent catalysts can be regarded intact in the present analysis, and the results herein can be compared with previous studies [15,16].

4.2. Global kinetics

The extinction–ignition profiles measured in the chemical flow reactor show typical shapes for CO oxidation over supported Pt catalysts including an ignition–extinction hysteresis [31]. The CO conversion changes rapidly from low to high in a narrow temperature interval when the temperature is increased, and vice versa, reflecting the

CO self-poisoning characteristics and competitive CO and O_2 adsorption [18,32,33]. Principally, the hysteresis is widened by heat and mass transfer characteristics, i.e., transport of heat generated by the exothermic oxidation reaction and mass transfer rates of the limiting reactant CO [34]. Here, the adiabatic temperature difference due to CO oxidation is about 20 °C, but the rigorous dilution with inert material lowered the practical temperature increase to 4°C, which makes thermal effects minor.

For the Pt/ceria catalyst, both the ignition and extinction of the reaction occur at lower temperatures for wet conditions as compared to dry conditions. The TOF increases from 0.015 s^{-1} in dry conditions, which is similar to TOFs reported by Meunier et al. [35], to 0.049 s^{-1} in wet conditions. However, the dependence on water concentration is very week. The water reaction order is −0.08, which close to zero. This shows that the water just being present is enough to alter the catalyst properties and/or promote the catalytic processes, at least when the H_2O concentration is between 0.8 and 2 vol.%. For CO oxidation at low temperatures under dry conditions, the rate-limiting step in the MvK mechanism is the desorption of product CO_2, which involves oxygen vacancy formation in the ceria surface close to the platinum [17]. When water is present, surface hydroxyls form that may promote the CO_2 desorption possibly by destabilising ceria lattice oxygen such that the overall activity increases. This is, however, not the only explanation for the improved CO oxidation activity. Also the apparent activation energy is different for wet and dry conditions, which indicates that another mechanistic step possibly involving another catalytic site becomes important. Although the apparent activation energy is higher during wet conditions, its magnitude is not too high to give appreciable CO oxidation activity at low temperatures. Further, the extrapolation of the Arrhenius curve would intercept with the vertical axis at higher values in the wet case indicating that the apparent pre-exponential factor is higher for wet conditions. This in turn suggests that the number of destabilised oxygen is higher and/or other, additional, sites are catalytically active. As will be discussed in more detail below, the *operando* DRIFTS results show that CO on ionic Pt, which is a spectator species under dry conditions, is not detected under wet conditions suggesting ionic Pt may be catalytically active under wet conditions. Further, pre-adsorbed water has an even stronger promoting effect on CO oxidation than continuously fed water at low conversions, i.e., at temperatures below about 75 °C. When water is not co-fed, only CO and O_2 adsorption compete. Thus, between the ignition temperature and the light-off temperature, i.e., the temperature region where CO coverage on platinum particles drops, the CO oxidation can proceed without competitive water adsorption. In effect, pre-adsorbed water promotes the processes discussed above responsible for the CO oxidation below the light-off temperature, but at around the light-off temperature, the CO oxidation reaction can proceed on the Pt particles without competing with water adsorption.

The Pt/alumina system is generally more prone to CO self-poisoning because the alumina cannot participate in the reaction in the same way as the reducible ceria as reflected also by the lower TOF for both dry and wet conditions. Clearly, water promotes the CO conversion, although less than for Pt/ceria. The ignition profile seems somewhat more smooth for wet conditions at low temperatures as compared to dry conditions suggesting that water loosens up the CO self-poisoning. Unlike for Pt/ceria, the H_2O reaction order shows that the concentration of water plays a role, even if water is not consumed in the reaction, indicating the possibility of involvement in the CO oxidation mechanism, for example via surface OH in the carboxylate route as has been described for unsupported platinum. As an example, for Pt(111), water has been suggested to promote the CO oxidation through hydrogen bonding with adsorbed O stabilising its transition state as well as offering a new reaction path proceeding via surface carboxylates (COOH) formed by the reaction between surface hydroxyls (OH) and adsorbed CO [9].

4.3. Surface properties and catalytic mechanisms

Analysis of the *in situ* and *operando* infrared spectroscopic results provides information about surface characteristics and adsorbed species and may shed some light on possible mechanisms too.

For Pt/ceria, comparing present wet conditions to reported dry conditions [15], the CO ad-species are redshifted by 32 cm^{-1} from 2107 to 2075 cm^{-1} and by 20 cm^{-1} from 2078 to 2058 cm^{-1} accompanied with intensity transfer from higher to lower wavenumber band. This suggests an increased electron backdonation from Pt to CO caused by an increased electron density of Pt due to ceria bound H_2O and OH species weakening the metal-support interaction as has been proposed for other Pt-based systems [36]. In addition, co-adsorption of CO and H_2O, likely also forming OH ad-species, on Pt can reduce the binding strength between CO and Pt [37] as well as lower the CO coverage, which effectively separates the adsorbed CO molecules from each other and leads to reduced CO-CO lateral interactions. The $\tilde{\nu}^{CO}_{lin}(Pt^{\delta+})$, at 2081 cm^{-1}, and $\tilde{\nu}^{CO}_{lin}(Pt^0)$ signatures are clear. Further CO binds strongly to Pt including oxidised Pt species favouring this assignment, especially as the $\tilde{\nu}^{CO}_{br}(Pt)$ band at lower wavenumbers is clearly present, although it is inherently weak. Possibly, the band could be caused by CO adsorbed on Pt kink sites bonded with OH species. This has been proposed for Pt/alumina [12], and has been suggested to be responsible for low-temperature CO oxidation activity in the presence of H_2O. The $\tilde{\nu}^{CO}_{lin}(Pt^{\delta+})$ band redshifts more upon increasing temperature than it blueshifts when the temperature is decreased again. This is a result of a relatively slow build-up of the CO coverage during extinction, which might be due to H_2O and OH ad-species blocking the CO adsorption. With increasing temperature, the $\tilde{\nu}^{CO}_{lin}(Pt^0)$ band decreases. This species has been reported to be an active species in the dry CO oxidation [38]. Interestingly, the $\tilde{\nu}^{CO}_{lin}(Pt^0)$ peak position is unaltered despite the varying intensity, i.e. varying CO coverage. It is unlikely that CO molecules bind to Pt sites and form a CO adsorption layer that is unaffected by the CO coverage. Instead, this peak position could signify CO ad-species that interact with H_2O, and the non-shifting $\tilde{\nu}^{CO}_{lin}(Pt^0)$ band implies that these CO ad-species are separated (isolated) by the H_2O and/or OH ad-species as has been proposed by Kizhakevariam et al. [39]. The initial small shifts of the $\tilde{\nu}^{CO}_{lin}$ bands during CO desorption from the water pre-exposed sample in our experiment support this suggestion.

Further, CO ad-species that under dry conditions have been considered to be spectator species, i.e., CO strongly bonded to ionic platinum present as a result of strong interaction between Pt and ceria [15], is not detectable under wet conditions. This indicates that ionic platinum is active when water is present. The ionic platinum clusters may become active when interacting with formed OH ad-species on the ceria surface either by promoting the MvK mechanism involving lattice ceria oxygen as described in the Introduction [15,17] or by OH ad-species that weaken the interaction between ceria and Pt as well as the CO-Pt bond. The CO_2 formation may then follow a route similar to the water promoted Mars-van Krevelen mechanism proposed by Wang et al. [40]. This mechanism includes a reaction pathway with low barriers in which CO adsorbs on Pt and then reacts with an OH species formed on ceria through water dissociation generating a COOH intermediate on Pt. The intermediate then reacts with another type of hydroxyl species formed with a lattice oxygen, $O_{lat}H$, at the interface forming CO_2 and H_2O. This step has been considered the rate-limiting step, and the vacancies created at the interface sites are healed by gas phase O_2 similar to dry CO oxidation [17], which closes the catalytic cycle.

The time-resolved spectra recorded during CO oxidation at 35 °C over Pt/ceria with pre-adsorbed H_2O show the presence of OH groups on ceria (present as a result of H_2O dissociation [41]). The negative peaks are associated with the suppression of the corresponding OH ad-species, which are still present on the surface after the pretreatment when the background spectra are taken [2]. The obvious decrease in intensity of the $\tilde{\nu}^{OH}_{mo}(Ce^{4+})$ band that seems to correlate with the increase in the intensity of the $\tilde{\nu}^{OH}_{br}(Ce^{3+})$ and $\tilde{\nu}^{OH}_{tr}(Ce^{4+})$ bands

is indicative of a reduction of the ceria. The simultaneous gradual decrease in CO_2 production suggests that the reduction of ceria, which likely is a removal of surface oxygen, decreases the catalytic activity. The growing $\tilde{\nu}_{lin}^{CO}$ bands that blueshift likely reflect the disappearance of adsorbed H_2O and OH as a result of the increasing CO coverage on Pt. However, compared to the CO ad-species present during H_2O co-feeding, both the $\tilde{\nu}_{lin}^{CO}(Pt^{\delta+})$ and $\tilde{\nu}_{lin}^{CO}(Pt^0)$ bands appear at higher wavenumbers probably due to less H_2O and/or OH coverage on Pt. Both the $\tilde{\nu}_{lin}^{CO}(Pt^{\delta+})$ and $\tilde{\nu}_{lin}^{CO}(Pt^0)$ species seem to participate in the CO oxidation reaction as they vanish in the active state of the catalyst. On the contrary, the $\tilde{\nu}_{lin}^{CO}(Pt^{2+})$ band exists even when the temperature reaches 213 °C, and thus appears to be spectator species similar as for dry CO oxidation [38,42]. The presence of the $\tilde{\nu}_{lin}^{CO}(Pt^{2+})$ band suggests that OH moieties may come not only from H_2O dissociation but also from the reaction between H_2O and O_2, which has been proposed to occur on platinum, for example on the Pt(111) surface.

For the Pt/alumina catalyst, it is clear that the presence of more prominent $\tilde{\nu}_{lin}^{CO}(Pt^0)$ bands demonstrate a less impact from the support as compared to ceria. Analogous to Pt/ceria, a clear redshift of 20-30 cm^{-1} is observed for CO ad-species in atop position accompanied by a lower linear to bridge ratio over Pt/alumina because of an increased electron backdonation to the $2\pi^*$ orbital of adsorbed CO. Moreover, a smaller redshift of 10 cm^{-1} is noticed for adsorbed CO in bridged configuration since H_2O and OH species are energetically less favoured to co-adsorb in an opposite-pointing dipole configuration with adjacent CO owing to a larger magnitude of the induced dipole for bridged CO adsorption. In stark contrast to Pt/ceria, an increase in temperature means an abrupt change in CO_2 production coupled with a drastic change in the intensities of $\tilde{\nu}_{lin}^{CO}$ and $\tilde{\nu}_{br}^{CO}$ bands. Simultaneously, a clear redshift of 7 cm^{-1} is observed for the $\tilde{\nu}_{lin}^{CO}(Pt^0)$ band at 2058 cm^{-1}, also stemming from a coverage effect. At 103 °C, the $\tilde{\nu}_{br}^{CO}$ band is completely vanished whereas minor $\tilde{\nu}_{lin}^{CO}(Pt^0)$ bands are visible. This can be explained by the presence of different Pt sites on the Pt particles that may have distinctly different catalytic activities. However, the intensity of the $\tilde{\nu}_{gas}^{CO_2}$ band during extinction changes less sharply than during ignition. At 83 °C, the CO_2 production substantially drops, which is correlated to the intensity change of the $\tilde{\nu}_{lin}^{CO}$ and $\tilde{\nu}_{br}^{CO}$ bands. Reaching 64 °C, the intensity of the $\tilde{\nu}_{gas}^{CO_2}$ band becomes hardly visible and the shoulder of the $\tilde{\nu}_{lin}^{CO}(Pt^0)$ band grows even stronger. Concurrently, when the Pt sites become CO poisoned, the activity of CO oxidation declines and the reduction of the oxidised Pt particles occurs leading to a redshift of the $\tilde{\nu}_{lin}^{CO}(Pt^0)$ bands. This can be discerned at the initial growth of the $\tilde{\nu}_{lin}^{CO}(Pt^0)$ band, here around 94 °C, of 1-2 cm^{-1} redshift. Further, a blueshift of around 5 cm^{-1} for the $\tilde{\nu}_{lin}^{CO}(Pt^0)$ band at 2059 cm^{-1} is observed caused by increasing CO coverage. It is interesting to observe the evolution of the CO species during the time-resolved measurements where CO desorbs from a water pre-exposed sample almost completely at 35 °C under Ar flow and then vanishes during the heating ramp. This is in stark contrast with CO desorption reported for dry CO oxidation over Pt/alumina where the intensity for $\tilde{\nu}_{lin}^{CO}$ bands remain almost unchanged after 2 h in He [43]. This is a clear indication that H_2O/OH weaken the bonding of CO with Pt, or even react with CO to form CO_2 via a COOH route on Pt particles, before forming a stable H_2O/OH layer on the Pt sites.

In summary, the spectroscopic results point in the direction that water promotes CO oxidation over Pt/ceria and Pt/alumina through different mechanisms. For Pt/ceria, water is suggested to promote the Mars-van Krevelen mechanism by destabilising ceria lattice oxygen such that its reaction with CO and/or desorption of product CO_2 is facilitated. This is supported by the observed reduction of ceria during CO oxidation indicating that ceria lattice oxygen takes part in the reaction. In addition, ionic platinum clusters seem to be catalytically active only in the case when water is co-fed. The zero dependence on water concentration and change in the slope of the Arrhenius curve supports the creation of another catalytic site that plays an important role in wet conditions. In contrast, for Pt/alumina, the water promotion is most likely a result of the direct interaction of water molecules with the CO adsorption layer on the Pt particles counteracting the CO self-poisoning effect. Likely hydroxyl ad-species form on the Pt particles weakening the CO-Pt bond. As the CO oxidation kinetics depend positively on the water concentration, the carboxylate route where OH and CO ad-species reacts as part of the CO oxidation mechanism as proposed by Gong et al. [9] cannot be excluded.

5. Conclusions

Kinetic and infrared spectroscopy measurements under *in situ* and *operando* conditions show that CO oxidation over Pt/ceria and Pt/alumina is promoted by water, although the underlying mechanisms appear to be different. In the case of Pt/ceria, hydroxyl groups formed on ceria sites in the close vicinity of the platinum particles promotes the Mars-van Krevelen mechanism responsible for the CO oxidation activity below the light-off temperature. In addition, the interaction of H_2O and/or OH groups significantly reduces the binding energy between, on the one hand, platinum and ceria, and, on the other hand, CO and Pt, turning ionic Pt clusters active for CO oxidation in presence of water. In contrast, CO oxidation over Pt/alumina follows the common Langmuir–Hinshelwood mechanism with a positive water dependence. Thus, water is suggested to not only affect the CO adsorption layer such that the interaction of CO with Pt becomes weaker but also form hydroxyl ad-species on platinum that may react with adsorbed CO promoting the proposed carboxylate route towards the formation of the product CO_2.

CRediT authorship contribution statement

Mengqiao Di: Writing – original draft, Investigation, Conceptualization. **Andreas Schaefer:** Writing – review & editing, Investigation. **Felix Hemmingsson:** Investigation. **Tamsin Bell:** Writing – review & editing, Supervision. **Yanyue Feng:** Investigation. **Magnus Skoglundh:** Writing – review & editing, Supervision, Funding acquisition. **David Thompsett:** Writing – review & editing, Supervision. **Per-Anders Carlsson:** Writing – review & editing, Supervision, Funding acquisition, Conceptualization.

Declaration of competing interest

The authors declare that they have no known competing financial interests or personal relationships that could have appeared to influence the work reported in this paper.

Acknowledgements

The authors thank the Swedish Research Council through the projects “Synergistic Development of X-ray Techniques and Applicable Thin Oxides for Sustainable Chemistry” (Dnr. 2017-06709) and “Infrared Spectroscopy in Time and Space” (Dnr. 2019-05528). Parts of this research were carried out at the Chalmers Materials Analysis Laboratory (CMAL) and we thank Stefan Gustafsson and Ludvig de Knoop for assistance. The work was carried out within the The Competence Centre for Catalysis is hosted by Chalmers University of Technology and financially supported by the Swedish Energy Agency (Project No. 52689-1) and the member companies Johnson Matthey, Perstorp, PowerCell Sweden, TRATON, Umicore, VAROPreem and Volvo Group.

Appendix A. Supplementary data

Supplementary material related to this article can be found online at https://doi.org/10.1016/j.apcato.2026.207113.

Data availability

Data will be made available on request.

References

[1] L. Lin, Y. Ge, H. Zhang, M. Wang, D. Xiao, D. Ma, Heterogeneous catalysis in water, JACS Au 1 (11) (2021) 1834–1848.

[2] P. Velin, M. Ek, M. Skoglundh, A. Schaefer, A. Raj, D. Thompsett, G. Smedler, P.A. Carlsson, Water Inhibition in Methane Oxidation over Alumina Supported Palladium Catalysts, J. Phys. Chem. C 123 (42) (2019) 25724–25737.

[3] P. Velin, C.-R. Florén, M. Skoglundh, A. Raj, D. Thompsett, G. Smedler, P.-A. Carlsson, Palladium dispersion effects on wet methane oxidation kinetics, Catal. Sci. Technol. 10 (16) (2020) 5460–5469.

[4] P. Velin, F. Hemmingsson, A. Schaefer, M. Skoglundh, K.A. Lomachenko, A. Raj, D. Thompsett, G. Smedler, P.A. Carlssonexhaus, Hampered PdO redox dynamics by water suppresses lean methane oxidation over realistic palladium catalysts, ChemCatChem 13 (17) (2021) 3765–3771.

[5] C.M. Kalamaras, S. Americanou, A.M. Efstathiou, "Redox" vs "associative formate with -OH group regeneration" WGS reaction mechanism on Pt/CeO_2: Effect of platinum particle size, J. Catalysis 279 (2) (2011) 287–300.

[6] X. Xie, Y. Li, Z.Q. Liu, M. Haruta, W. Shen, Low-temperature oxidation of CO catalysed by Co_3O_4 nanorods, Nature 458 (7239) (2009) 746–749.

[7] H.F. Wang, R. Kavanagh, Y.L. Guo, Y. Guo, G.Z. Lu, P. Hu, Structural origin: Water deactivates metal oxides to CO oxidation and promotes low-temperature CO oxidation with metals, Angew. Chem. - Int. Ed. 51 (27) (2012) 6657–6661.

[8] J.S. Filhol, M. Neurock, Elucidation of the electrochemical activation of water over pd by first principles, Angew. Chem. - Int. Ed. 45 (3) (2006) 402–406.

[9] X.Q. Gong, P. Hu, R. Raval, The catalytic role of water in CO oxidation, J. Chem. Phys. 119 (12) (2003) 6324–6334.

[10] T.E. Shubina, C. Hartnig, M.T. Koper, Density functional theory study of the oxidation of CO by OH on Au(110) and Pt(111) surfaces, Phys. Chem. Chem. Phys. 6 (16) (2004) 4215–4221.

[11] C. Wang, X.K. Gu, H. Yan, Y. Lin, J. Li, D. Liu, W.X. Li, J. Lu, Water-mediated mars-van krevelen mechanism for CO oxidation on ceria-supported single-atom Pt_1 catalyst, ACS Catal. 7 (1) (2017) 887–891.

[12] Y. Chen, Y. Feng, L. Li, J. Liu, X. Pan, W. Liu, F. Wei, Y. Cui, B. Qiao, X. Sun, X. Li, J. Lin, S. Lin, X. Wang, T. Zhang, Identification of active sites on high-performance Pt/Al_2O_3 catalyst for cryogenic CO oxidation, ACS Catal. 10 (15) (2020) 8815–8824.

[13] A.M. Abdel-Mageed, S. Eckle, D. Widmann, R. Behm, Water assisted dispersion of ru nanoparticles: The impact of water on the activity and selectivity of supported Ru catalysts during the selective methanation of CO in CO2-rich reformate, J. Catalysis 335 (2016) 79–94.

[14] T. Mizushima, K. Tohji, Y. Udagawa, A. Ueno, An EXAFS and IR study of the CO adsorption-induced morphology change in ruthenium catalysts, J. Am. Chem. Soc. 112 (22) (1990) 7887–7893.

[15] M. Di, K. Simmance, A. Schaefer, Y. Feng, F. Hemmingsson, M. Skoglundh, T. Bell, D. Thompsett, L.I. Ajakaiye Jensen, S. Blomberg, P.A. Carlsson, Chasing PtOx species in ceria supported platinum during CO oxidation extinction with correlative operando spectroscopic techniques, J. Catalysis 409 (2022) 1–11.

[16] M. Di, A. Schaefer, F. Hemmingsson, T. Bell, Y. Feng, M. Skoglundh, D. Thompsett, P.-A. Carlsson, Why nitrogen oxide inhibits CO oxidation over highly dispersed platinum ceria catalysts, Catal. Today (2023) 114394.

[17] N. Bosio, M. Di, M. Skoglundh, P.-A. Carlsson, H. Grönbeck, Interface reactions dominate low-temperature CO oxidation activity over Pt/CeO2, J. Phys. Chem. C 126 (38) (2022) 16164–16171.

[18] P.-A. Carlsson, L. Österlund, P. Thormählen, A. Palmqvist, E. Fridell, J. Jansson, M. Skoglundh, A transient in situ FTIR and XANES study of CO oxidation over Pt/Al_2O_3 catalysts, J. Catal. 226 (2) (2004) 422–434.

[19] W. Rasband, Imagej, 2021, URL https://imagej.nih.gov/ij/.

[20] C. Zhang, J. Gustafson, L.R. Merte, J. Evertsson, K. Norén, S. Carlson, H. Svensson, P.-A. Carlsson, An in situ sample environment reaction cell for spatially resolved X-ray absorption spectroscopy studies of powders and small structured reactors, Rev. Sci. Instrum. 86 (3) (2015) 033112.

[21] P. Velin, U. Stenman, M. Skoglundh, P.A. Carlsson, Portable device for generation of ultra-pure water vapor feeds, Rev. Sci. Instrum. 88 (11) (2017) 115102.

[22] L. Nie, D. Mei, H. Xiong, B. Peng, Z. Ren, X.I.P. Hernandez, A. DeLaRiva, M. Wang, M.H. Engelhard, L. Kovarik, A.K. Datye, Y. Wang, Activation of surface lattice oxygen in single-atom Pt/CeO_2 for low-temperature CO oxidation, Science 358 (6369) (2017) 1419–1423.

[23] P. Bazin, O. Saur, J.C. Lavalley, M. Daturi, G. Blanchard, FT-IR study of CO adsorption on Pt/Ceo_2: Characterisation and structural rearrangement of small Pt particles, Phys. Chem. Chem. Phys. 7 (1) (2005) 187–194.

[24] C. Lentz, S.P. Jand, J. Melke, C. Roth, P. Kaghazchi, DRIFTS study of CO adsorption on Pt nanoparticles supported by DFT calculations, J. Mol. Catal. A: Chemical 426 (2017) 1–9.

[25] E. Becker, P.-A. Carlsson, L. Kylhammar, M.A. Newton, M. Skoglundh, In situ spectroscopic investigation of low-temperature oxidation of methane over alumina-supported platinum during periodic operation, J. Phys. Chem. C 115 (4) (2011) 944–951.

[26] J. Raskó, CO-induced surface structural changes of Pt on oxide-supported Pt catalysts studied by DRIFTS, J. Catal. 217 (2) (2003) 478–486.

[27] C. Binet, M. Daturi, J.C. Lavalley, IR study of polycrystalline ceria properties in oxidised and reduced states, Catal. Today 50 (2) (1999) 207–225.

[28] A. Badri, C. Binet, J.C. Lavalley, An FTIR study of surface ceria hydroxy groups during a redox process with H2, J. Chem. Soc. - Faraday Trans. 92 (23) (1996) 4669–4673.

[29] M. Inoue, M. Kimura, T. Inui, Transparent colloidal solution of 2 nm ceria particles, Chem. Commun. (11) (1999) 957–958.

[30] H.P. Klug, L.E. Alexander, X-Ray Diffraction Procedures: For Polycrystalline and Amorphous Materials, John Wiley & Sons, New York, 1974.

[31] P.-A. Carlsson, M. Skoglundh, Low-temperature oxidation of carbon monoxide and methane over alumina and ceria supported platinum catalysts, Appl. Catal. B: Environ. 101 (3–4) (2011) 669–675.

[32] P.-A. Carlsson, P. Thormählen, M. Skoglundh, H. Persson, E. Fridell, E. Jobson, B. Andersson, Periodic control for improved low-temperature catalytic activity, Top. Catal. 16 (1) (2001) 343–347.

[33] P.-A. Carlsson, M. Skoglundh, E. Fridell, E. Jobson, B. Andersson, Induced low temperature catalytic ignition by transient changes in the gas composition, Catal. Today 73 (3–4) (2002) 307–313.

[34] P.-A. Carlsson, M. Skoglundh, P. Thormählen, B. Andersson, Low-temperature CO oxidation over a Pt/Al_2O_3 monolith catalyst investigated by step-response experiments and simulations, Top. Catal. 30 (1) (2004) 375–381.

[35] F.C. Meunier, L. Cardenas, H. Kaper, B. Šmíd, M. Vorokhta, R. Grosjean, D. Aubert, K. Dembélé, T. Lunkenbein, Synergy between metallic and oxidized Pt sites unravelled during room temperature CO oxidation on Pt/ceria, Angew. Chem. Int. Ed. 60 (7) (2021) 3799–3805.

[36] P.V. Menacherry, G.L. Haller, The effect of water on the infrared spectra of CO adsorbed on Pt/K L-zeolite, Catal. Lett. 1997 44:3 44 (3) (1997) 135–144.

[37] S. Zhao, F. Chen, S. Duan, B. Shao, T. Li, H. Tang, Q. Lin, J. Zhang, L. Li, J. Huang, N. Bion, W. Liu, H. Sun, A.Q. Wang, M. Haruta, B. Qiao, J. Li, J. Liu, T. Zhang, Remarkable active-site dependent H_2O promoting effect in CO oxidation, Nat. Commun. 10 (1) (2019) 1–9.

[38] K. Ding, A. Gulec, A.M. Johnson, N.M. Schweitzer, G.D. Stucky, L.D. Marks, P.C. Stair, Identification of active sites in CO oxidation and water-gas shift over supported pt catalysts, Science 350 (6257) (2015) 189–192.

[39] N. Kizhakevariam, X. Jiang, M.J. Weaver, Infrared spectroscopy of model electrochemical interfaces in ultrahigh vacuum: The archetypical case of carbon monoxide/water coadsorption on Pt(111), J. Chem. Phys. 100 (9) (1994) 6750–6764.

[40] Y. Wang, J. Ma, X. Wang, Z. Zhang, J. Zhao, J. Yan, Y. Du, H. Zhang, D. Ma, Complete CO oxidation by O_2 and H_2O over Pt-$CeO_{2-\delta}$ MgO following langmuir-hinshelwood and mars-van krevelen mechanisms, respectively, ACS Catal. 11 (19) (2021) 11820–11830.

[41] S. Fuente, M.M. Branda, F. Illas, Role of step sites on water dissociation on stoichiometric ceria surfaces, Theor. Chem. Accounts 131 (3) (2012) 1–7.

[42] F.C. Meunier, Relevance of IR spectroscopy of adsorbed CO for the characterization of heterogeneous catalysts containing isolated atoms, J. Phys. Chem. C 125 (40) (2021) 21810–21823.

[43] F.C. Meunier, T. Elgayyar, K. Dembélé, H. Kaper, Stability of Pt-Adsorbed CO on Catalysts for Room Temperature-Oxidation of CO, Catalysts 12 (5) (2022) 532.